Title
Observational Evidence for Both Aerosol-Induced Invigoration and Enervation

Journal
Journal of Geophysical Research: Atmospheres, 131(14)

ISSN
2169-897X

Authors
Pimperl, Hallie E
Igel, Adele M

Publication Date
2026-07-28

DOI
10.1029/2025jd046280

Observational Evidence for Both Aerosol-Induced Invigoration and Enervation

Hallie E. Pimperl[1], Adele M. Igel[1,2]

[1]Atmospheric Sciences Graduate Group, University of California, Davis, Davis, CA 95616, USA

[2] Department of Land, Air, and Water Resources, University of California, Davis, Davis, CA 95616, USA

Corresponding author: Hallie E. Pimperl (hepimperl@ucdavis.edu)

Key Points:

- The likelihood of observing an invigoration effect increases in environments which promote high supersaturations.
- The likelihood of detecting an enervation effect strengthens in environments which promote entrainment.
- The observational results of this study are largely qualitatively consistent with previous modeling studies.

Abstract

Previous modeling studies have shown a connection between higher aerosol concentrations and heightened updraft speeds in convective clouds, an effect known as aerosol-induced invigoration. Observational evidence of this phenomenon, however, is inconclusive. We seek to provide a statistically robust, observational assessment of the effects of aerosol invigoration on isolated, developing, midlatitude, deep convective updraft speeds. This study uses geostationary satellite data to track approximately 225 storms over the Southern Great Plains. We show using cloud resolving model simulations that convective updraft speeds are proportional to the cloud top rise rate. After controlling for meteorology, the results suggest that high concentrations of small aerosol particles can invigorate convection, whereas accumulation mode particles may enervate updrafts at mid to upper levels of the storms. The statistical significance of an invigoration effect increases under environmental conditions that promote high supersaturation (strong updrafts, extensive warm phase regions), while the significance of an enervation response is enhanced under conditions that promote entrainment (high wind shear, lower cloud bases). These results are largely in agreement with many past modeling studies but have not been seen previously in observations. Our findings suggest that future efforts in the field should reject the framework of invigoration *or* enervation and instead focus on the specific conditions under which each response is expected.

Plain Language Summary

While modeling studies have previously linked greater amounts of aerosol particles to changes in storm updraft speeds, the difficulty in detecting such a relationship using observations has largely hindered the ability to validate this phenomenon. To bridge this gap, this study uses satellite data, ground-based aerosol measurements, and robust statistical methods to detect aerosol influences on thunderstorm cloud tops over Oklahoma. Ultimately, we cannot prove that aerosols have altered the rise of cloud tops. We do, however, uncover specific conditions that can improve the ability to detect an aerosol effect. We find that high concentrations of aerosols could strengthen the rise of the cloud top under high supersaturations but weaken its ascent with greater dilution of the surrounding air. These findings are largely consistent with the existing literature. Thus, we emphasize that polluted storms are equally likely to see a faster or slower rise in their cloud tops and that their specific conditions will dictate which response can be expected.

1 Introduction

The aerosol invigoration effect refers to the phenomenon where an increase in aerosol concentrations amplifies convective cloud updraft speeds (Altaratz et al., 2014; Andreae et al., 2004; Grabowski, 2018; Rosenfeld et al., 2008; Tao et al., 2012; Varble et al., 2023). Previous studies have hypothesized two modes of invigoration: cold-phase invigoration and warm-phase invigoration. Cold-phase invigoration occurs in deep convection when precipitation is suppressed under polluted conditions, delaying condensate unloading past the freezing level. Additional latent heat is released upon freezing, followed by instantaneous unloading of condensate – both of which provide a buoyancy boost to the polluted storm (Rosenfeld et al., 2008). Warm-phase invigoration similarly relies on additional latent heat release but through an increase in the condensation rate, at levels typically near cloud base and/or through secondary activation of ultrafine particles further aloft. The additional latent heat released by this process will, again, feed the buoyancy of the storm and "invigorate" the clouds (Fan et al., 2007, 2018; Grabowski and Morrison, 2016; Koren et al., 2014).

The proposed magnitude of an aerosol invigoration effect on convective updraft speeds is widely debated. Theoretical calculations by Igel and van den Heever (2021) suggest that warm-phase invigoration is possible, albeit at magnitudes much smaller than is suggested by Fan et al. (2018). (Romps et al., 2023), however, argues that warm-phase invigoration should not "have any practically significant impacts on cloud buoyancy and updraft speeds." Other studies have suggested that if polluted storms loft substantially more condensate upwards, enervation, or weakening, of the convection is possible (Igel and van den Heever, 2021), particularly if the effects of entrainment are taken into account (Peters et al., 2023). Igel and van den Heever (2021) additionally demonstrate that if condensate loading is realistically considered, the magnitude of cold-phase invigoration should be much less than is suggested by Rosenfeld et al. (2008).

Several observational works have previously shown evidence of an aerosol-induced invigoration signal, typically using updraft strength proxies, such as cloud top height or cloud top temperature (Fan et al., 2018; Koren et al., 2012; Li et al., 2011; Lin et al., 2006; Storer et al., 2014). Yet other studies suggest that imperfect methodologies raise doubts about the viability and importance of these observed signals (Grabowski, 2018; Öktem et al., 2023; Varble, 2018). Both Varble (2018) and Grabowski (2018) argue that small changes to environmental properties can produce similar modifications to cloud development as those resulting from enhanced aerosol concentrations. Because of this, Grabowski (2018) argues that it is not possible to separate meteorological effects on cloud properties from aerosol factors using observations. Observational evidence of invigoration is further disputed due to the use of proxies for both aerosol and updraft speed, unincorporated influences of cloud life cycle on updraft evolution, improper accountability of meteorological impacts, and an obscurity in how the term invigoration is defined (Altaratz et al., 2014; Fan et al., 2018; Igel and van den Heever, 2021; Koren et al., 2012; Li et al., 2011; Lin et al., 2006; Tao et al., 2012; Varble, 2018; Varble et al., 2023; Veals et al., 2022).

In this study, we provide an observational assessment on the effects of increased aerosol concentrations on a deep convective updraft proxy called the cloud top rise rate. To test the null hypothesis, that aerosol invigoration or enervation is not significant, we look for either signal under conditions in which we believe it should be most easily detected – namely, in isolated, developing storms. We aim to avoid the shortcomings of previous observational studies by synthesizing recommendations from the field regarding proxy use and proper environmental control (Altaratz et al., 2014; Fan et al., 2025; Tao et al., 2012; Varble, 2018; Varble et al., 2023). While we do not claim definitive proof of aerosol-induced invigoration or enervation in our results, the following sections will show evidence of both invigoration and enervation under different conditions that is largely consistent with the previous modeling studies.

2 Methods

2.1 Tracking

The GOES-16 satellite provides stationary coverage of the contiguous United States every five minutes (Schmit et al., 2017). Using GOES-16's clean window brightness temperature (Band 13), cloud top phase, and cloud mask products, we track isolated, developing, deep convective cloud tops for seven years (2017-2024) from May to September within a 5°x5° region centered on the Atmospheric Radiation Measurement (ARM) Southern Great Plains (SGP) Central Facility site (https://registry.opendata.aws/noaa-goes, accessed on 07/04/2025). We track isolated, developing storms because they are most applicable to the parcel theory framework upon which the aerosol-induced invigoration theories are built (Igel and van den Heever, 2021; Rosenfeld et al., 2008) and should be mostly free of feedbacks that develop later in the storm lifecycle.

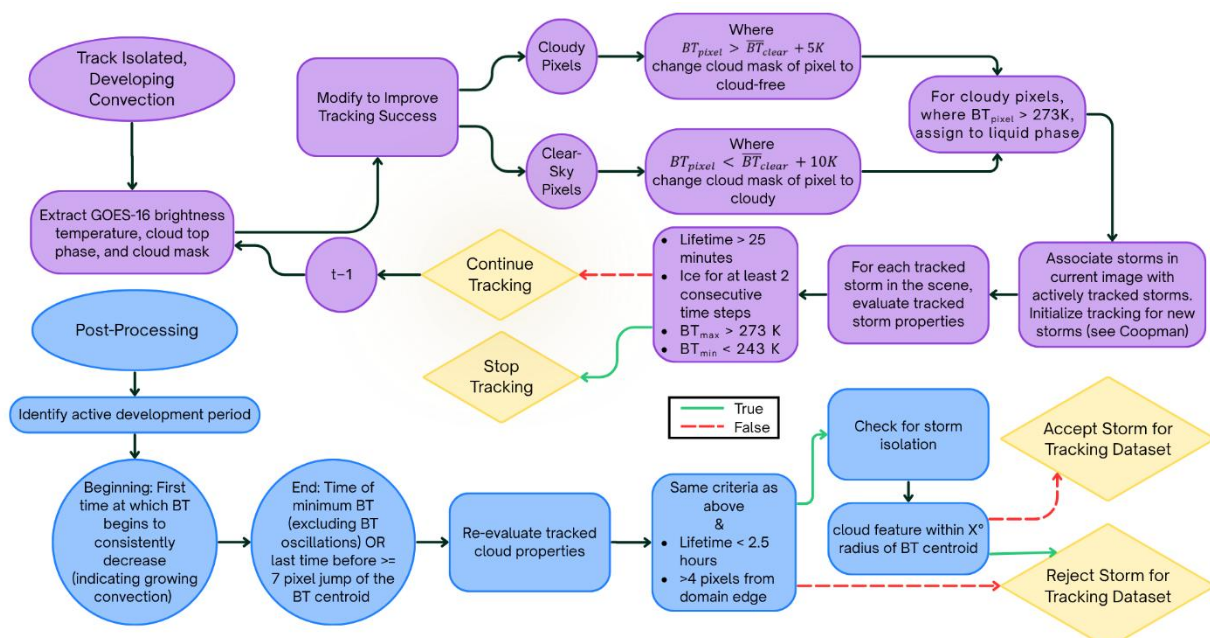

Figure 1. Flowchart showing how storms are tracked and evaluated to form the final tracking dataset. The tracking process is shown in purple, with the quality control decisions of the post-processing stage shown in blue. Diamonds indicate decision points in the algorithm.

To improve tracking success, modifications to the GOES-16 data products are made (see Figure 1). A cloudy pixel is changed to cloud-free if its brightness temperature is *greater* than 5 K above the clear-sky mean, while a clear-sky pixel is changed to cloudy if its brightness temperature is 10 K *below* the clear-sky mean. While these reassignments may not always be appropriate, the change allows us to remove very shallow clouds from the cloud mask that would not be considered part of the developing deep convection. Any cloudy pixels with brightness temperatures above 273 K are assigned to the liquid phase.

The tracking algorithm used in this study is adapted from Coopman et al. (2020) and follows brightness temperature minimums between timesteps. The algorithm works by assigning unique labels to adjacent cloudy pixels to initialize cloud features. It then tracks the development of these features backward in time by confirming that overlap exists between cloudy pixels in the current image and cloudy pixels in the previous images. (See Coopman et al. (2020) for more details.) Tracked storms are written to a file if: their lifetime is greater than or equal to five timesteps (25 minutes), the cloud top phase is icy for at least two timesteps, the minimum brightness temperature is 243 K or less, and the maximum brightness temperature is 273 K or greater. The beginning of the active development phase is marked as the first time at which the brightness temperature consistently decreases towards its minimum, meaning it does not increase in temperature again between any two points. Usually, the start of active development is triggered by the first tracked timestep, but sometimes the above criterion is necessary to eliminate time during which shallow convection is oscillating before reaching the level of free convection and developing rapidly. The end of the developing phase is detected when:

- The 3-point smoothed brightness temperature begins to increase again after the minimum brightness temperature is reached, *or*
- The brightness temperature centroid has jumped more than 7 pixels from the previous timestep, possibly indicating the development of a new convective core.

Tracking timesteps that are outside of the active development period are removed from a storm's time series. Storms whose lifetimes exceed 2.5 hours, whose brightness temperature centroids come within 4 pixels of the domain edge, or whose attributes within the active development period no longer meet the above criteria are removed from the dataset. To check for isolation, we note the distance to the nearest neighboring cloud feature. After applying these quality control measures, we have 86 tracked storms with no neighboring cloud features within 0.50° and 225 tracked storms with no neighboring cloud features within 0.25°.

2.2 Cloud Top Rise Rate

We use the tracked storms' cloud top rise rate (CTRR) as a proxy for updraft speed due to its inherent link to the convective development of the storm. CTRR is calculated by performing a one-dimensional, linear interpolation on the High Resolution Rapid Refresh (HRRR) model's temperature and height profiles to match the tracked brightness temperature minimums along the mean profile. Such a procedure assumes that the observed clean window brightness temperature is equivalent to the actual cloud top temperature. We believe this to be a reasonable assumption because cloud tops are at mid- to upper levels during their most rapid period of development.

The cloud top rise rate is calculated in two ways: as the maximum 25-minute moving window of mean CTRR (CTRRMM) and as the maximum 5-minute CTRR (CTRRMAX).

2.3 Meteorological Context

To provide the meteorological context for each tracked storm, we extract HRRR environmental variables at the hour immediately prior to the initiation of convection (see Table A1 in the Appendix for details). Other quantities, such as the horizontal wind shear, the lifting condensation level (LCL), etc., are derived from the HRRR model output (https://rapidrefresh.noaa.gov/hrrr/, accessed on 07/15/2025).

We perform a multiple linear regression (MLR) between the environmental variables and CTRR (see Table A2 in the Appendix) to filter for environmental influences in a statistically robust way, as common controlling practices, such as binning of meteorological variables, can fail to unconditionally remove environmental influences and can allow relationships between aerosol and the environment to persist between bins (Fan et al., 2018; Koren et al., 2012; Li et al., 2011; Lin et al., 2006; Grabowski, 2018; Varble, 2018; Varble et al., 2023). Therefore, the predicted CTRR in the regression is the contribution of meteorology to the growth of the tracked storms, while the residuals represent the remaining influences on the rise rates, including those driven by aerosols.

The linear regression model used in this study is from SciKitLearn's Linear Regression Module. Regression models are generated for each of the two dependent variables (CTRRMM and CTRRMAX). The number of predictors used in the model is determined by the size of the dataset, corresponding to roughly 10 observations per predictor. Predictors are selected to produce the highest adjusted-R^2 values to explain as much of the environmental influence as possible. To increase the robustness of the adjusted-R^2 values, we bootstrap the data by resampling the dataset 1,000 times (with replacement) and average over all 1,000 of the resulting adjusted-R^2 values.

2.4 Aerosol Invigoration Signal

The SGP ARM site provides ground-based aerosol measurements from the Scanning-Mobility Particle Sizer (SMPS) instruments at a five minute resolution (Kuang et al., 2021a, b). The (regular) SMPS data operates in the range of 8 nm - 500 nm, and the nano SMPS optimally detects within a size range of 2.5 nm - 65 nm. The aerosol data is obtained in the five minutes immediately prior to the initiation of the storm. The aerosols are binned into the following size ranges to evaluate the role of aerosol diameter in aerosol-induced invigoration:

- Nanoscale: 2.5 nm – 65 nm (nano SMPS)
- Nucleation Mode: 2.5 nm – 10 nm (nano SMPS)
- Aitken Mode: 10 nm – 100 nm (regular SMPS)
- Accumulation Mode: 100 nm – 500 nm (regular SMPS)

To conduct an analysis of the potential for aerosol invigoration, we compare the aerosol concentration data for each activation mode to the change in the kinetic energy of the storm. The observed kinetic energy (KE) of a deep convective storm is a linear combination of some reference kinetic energy ($\mathrm{KE_{ref}}$) that would be expected based on the thermodynamic environment plus additional kinetic energy due to aerosol impacts that are not accounted for in the thermodynamic environment ($\Delta\mathrm{KE_{aero}}$), that is $\mathrm{KE} = \mathrm{KE_{ref}} + \Delta\mathrm{KE_{aero}}$. In our study, we write this equation as $\frac{1}{2}\mathrm{CTRR_{obs}}^2 = \frac{1}{2}\mathrm{CTRR_{pred}}^2 + \Delta\mathrm{KE_{res}}$, where $\mathrm{CTRR_{obs}}$ is derived from the tracking,

$CTRR_{pred}$ represents the cloud top rise rates predicted by the regression model, and ΔKE_{res} contains aerosol influences and any unattributed contributions to the rise rates. We choose to reframe the question in terms of kinetic energy because, under the idealization of parcel theory, ΔKE_{res} is nearly independent of the environment in which the storm develops (Igel and van den Heever, 2021). This independence arises because, for two storms developing in the same environment, the difference in buoyancy at any level is proportional to the density temperature difference of the parcels. That said, the incomplete ability of parcel theory to predict storm updraft speeds, plus other influences not considered in parcel theory, such as wind shear and entrainment, as well as the boundary conditions (cloud base temperature, storm depth), will affect the additional energy given to the storm by increased aerosol concentrations. While the kinetic energy framework by no means completely separates the influence of the environment on the magnitude of an aerosol signal, we believe that its use will better detect aerosol influences on storm dynamics than updraft speed alone.

2.5 Approximation to Updraft Speed

In this study, we assume that CTRR is a strong proxy for the updraft speed in the convective core. To test this assumption, we use the DOE LASSO CACTI model simulation suite (Gustafson et al., 2017). We track clouds using the same tracking procedures described in Section 2.1. The cloud top height for the CTRR proxy in the LASSO simulations is indexed at the point of minimum brightness temperature *and* wherever the cloud mixing ratio is nonzero. Updraft speed (w) is identified in the model at the location of the maximum updraft speed within 1 km from the designated cloud top in the minimum brightness temperature column. Thirty simulations of Argentinian summer convection are used for the tracking, with model output at a 5-minute resolution. Because clean window brightness temperatures are not available in the LASSO dataset, the brightness temperature criteria that signal the beginning and end of the active phase of development are replaced with corresponding height criteria – namely, that the minimum cloud top height must be less than or equal to 5 km and the maximum must exceed 7 km. In total, we tracked and retained 77 storms.

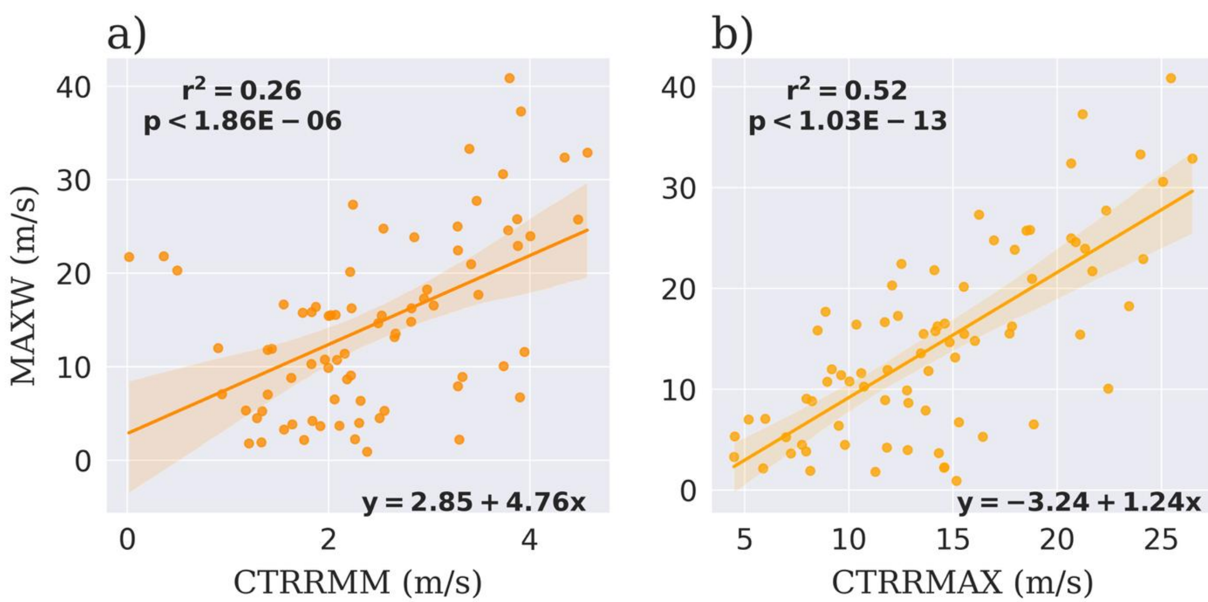

Figure 2. Relationship of CTRMM (a) and CTRRMAX (b) to the maximum vertical velocity (MAXW), with corresponding r^2, p-values, and least-squares fit of the simple linear regressions.

We calculate the two dependent variables for cloud top rise rate, CTRRMM and CTRRMAX, from the LASSO data. The tracked *w* values are used to calculate MAXW, which is the largest increase in *w* between two timesteps. (A similar calculation was performed to find CTRRMM's *w* counterpart, but MAXW was found to have a stronger relationship to both rise rates.) A simple linear regression is performed to establish the relationship between CTRRMM and CTRRMAX with MAXW, as shown in Figure 2. We find a moderate association between CTRRMM and maximum updraft speed (r^2=0.26) and a stronger association between CTRRMAX and maximum updraft speed (r^2=0.52). We argue that the relationships between MAXW and the CTRR variables are strong enough to use CTRR as a proxy for updraft speed in this study. Because the intercept of the best fit lines is small compared to the range of the data, the kinetic energy residuals (ΔKE_{res}) when using MAXW versus CTRR differ approximately by a scaling factor. Therefore, the two dependent variables, MAXW and CTRR, can be used almost interchangeably in the residual analysis framework, and we present only the results using CTRR in the remainder of the study.

3 Results

3.1 Storm Characteristics

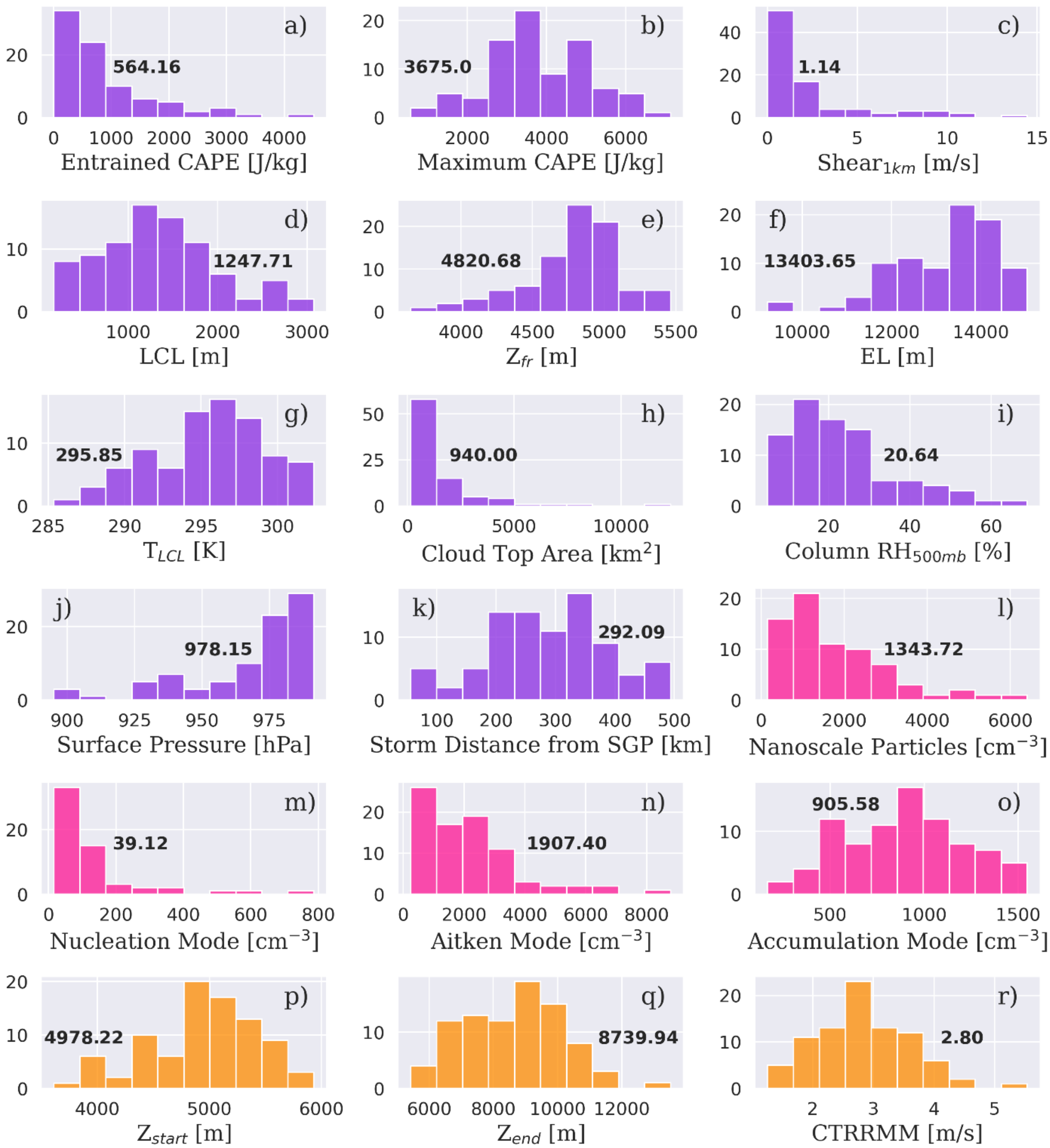

Figure 3. Histograms of important environmental considerations (a-k), aerosol mode concentrations (l-o), and attributes of CTRRMM (p-r). The median value of each distribution is displayed in each subplot and bins are fixed at 10.

The meteorological variables included as predictors in the MLR models and/or discussed in the following analysis are shown in Figure 3, along with the aerosol mode distributions and characteristics of the CTRRMM updraft proxy. As expected, the atmosphere prior to convection is highly unstable, indicated by the high levels of maximum CAPE (Figure 3b). Figure 3 shows a median LCL of 1.3 km (Fig. 3d) and a median EL (equilibrium level) of 13.40 km (Fig. 3f), indicating that storms can achieve significant depth. Deeper storms may experience greater environmental mixing over their prolonged extent. Indeed, we see a median entrained CAPE (ECAPE, following (Peters et al., 2023)) of 564 J/kg (Figure 3a), suggesting potentially strong dilution of the updraft core. Finally, note that the CTRMM window extends between ~5-9 km (Figure 3p,q), which is primarily above the median freezing level (Figure 3e).

Figure 3c shows relatively weak low-level wind shear, with a median 0-1km shear of 1.1 m/s, indicating a potential lack of low-level synoptic ascent and supporting our conjecture that the storms freely convect (Markowski and Richardson, 2010). Weak values of low-level wind shear also typically support single cell convection rather than more organized systems (Baidu et al., 2022; Markowski and Richardson, 2010). Indeed, the median cloud top area for the storms in Figure 3h falls around 940 km^2, suggesting that the storms are likely isolated. We focus on isolated storms because, as can be seen in Figure 4, the average adjusted-R^2 values, which indicate the ability of the environmental properties to predict CTRR, increase with strengthening degree of isolation. This is an encouraging result because it means that the environments of more isolated storms can predict the cloud top rise rates better than the environments of less isolated storms. It suggests that, consistent with our expectations, storm development is influenced by neighboring storms that are not accounted for in the list of predictors. The results of Figure 4 additionally reveal that CTRRMM consistently outperforms its CTRRMAX counterpart in predictability. We therefore expect that CTRRMM will be better able to uncover an aerosol influence on the cloud top rise rate, should such a signal exist. Thus, we focus only on the CTRRMM results of the 0.50° isolation dataset in the following analysis (see Appendix B for further statistical assessment).

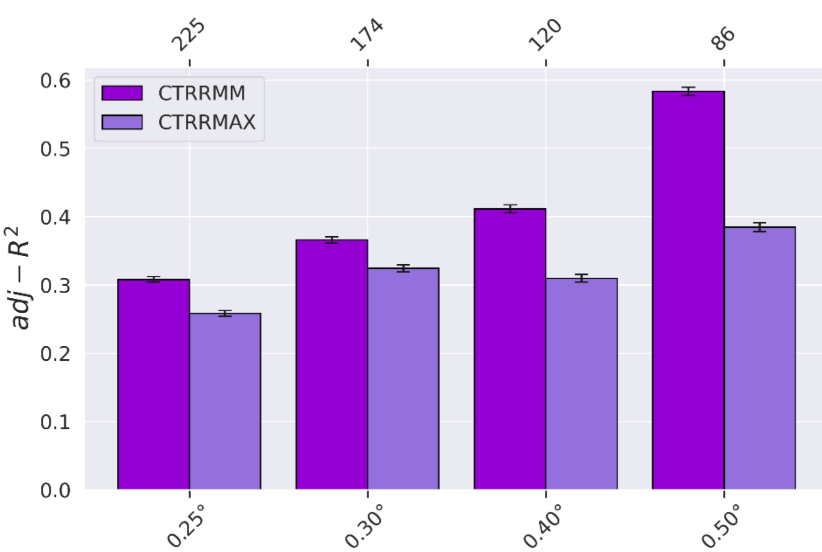

Figure 4. Bar graph of the average, bootstrapped adj-R^2 regression fit for each isolation case for CTRRMM (left) and CTRRMAX (right). The number of tracked storms in each dataset is listed above each bar pair. All mean adj-R^2 values, including confidence intervals of the bootstrapped adj-R^2 samples (shown as error bars), are considered significant at the 99% confidence level.

3.2 CTRR Responses to Aerosol Modes

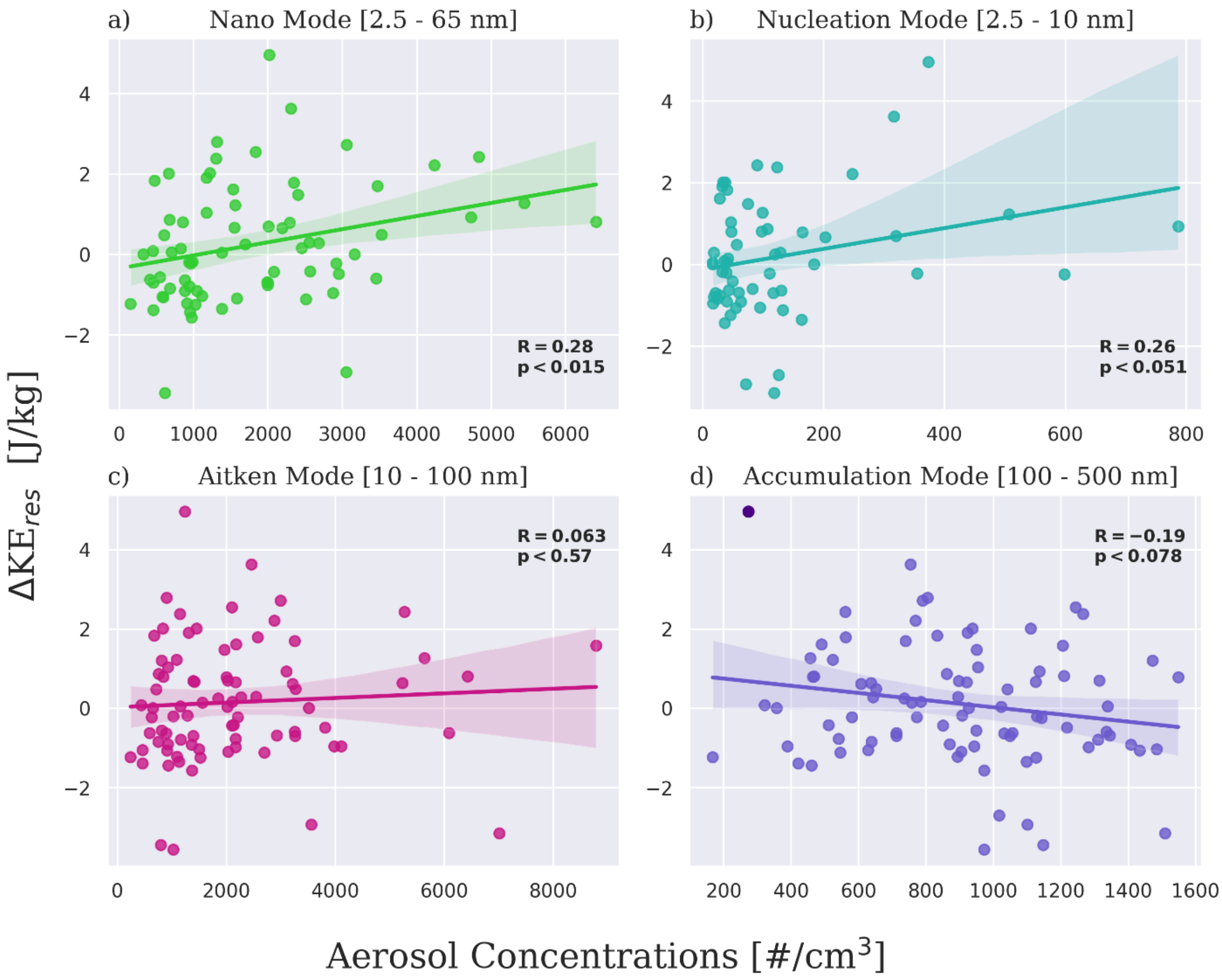

Figure 5. Scatterplot of aerosol number concentration against ΔKE_{res} based on aerosol activation mode, with shaded regions representing the 95% confidence interval of the proposed trendline. Statistical metrics of the relationship, including correlation and statistical confidence are displayed on each graph. A ΔKE_{res} outlier is highlighted in dark purple for the accumulation mode particles in 5d.

To analyze the contribution of aerosol to the kinetic energy of the tracked storms, we correlate ΔKE_{res} with a given aerosol activation mode (Figure 5). We remove outlying aerosol concentrations (>700 cm^{-3} from the nearest non-outlier) to prevent their existence from controlling the slope of the best-fit line. The maximum number of outliers is five, for the nanoscale mode.

Nanoscale particle concentrations show a statistically significant, positive trend in ΔKE_{res} for increasing aerosol concentration (Figure 5a). (Statistical significance throughout this paper refers to the 95% confidence level unless stated otherwise). Despite neither mode achieving statistical significance, the nucleation mode aerosol concentrations show an increasing trend in ΔKE_{res} with increasing aerosol concentration (Figure 5b), while the accumulation mode particles show a trending decrease in ΔKE_{res} (Figure 5d). However, Figure 5d also shows an outlier in ΔKE_{res}, highlighted in dark purple, that controls the weakening signal for heightened accumulation mode concentrations ($R = -0.19$, $p < 0.08$ to $R = -0.13$, $p < 0.24$ with the outlier removed). The transition between the opposing trends occurs within the Aitken mode (Figure 5c). The data, therefore, suggest that invigoration may occur only when there is an enhancement in concentration of only the smallest aerosol particles.

A recent study by Wang et al. (2025) saw qualitatively similar trends as in Figure 5. The study found significant associations between an increase in echo top height and greater aerosol loadings for aerosol diameters between 3-3000nm and 8-3000nm. When correlating the total concentration of aerosol particles with ΔKE_{res}, as in Wang et al. (2025), our dataset does not achieve statistical significance. However, because fine aerosol particles typically dominate total aerosol concentrations, the results of Figure 5a,b and Wang et al. (2025) are likely similar. The results are also consistent with Fan et al. (2018) who proposed that ultrafine particles could drive invigoration. This hypothesis was based on observational analysis that was not statistically significant (Fan et al., 2018; Öktem et al., 2023) but supported by modeling results. The study proposed that efficient warm rain production suppressed condensation until heightened supersaturations activated smaller ultrafine particles, enhancing the integrated droplet surface area and secondarily increasing the condensation rate.

Wang et al. (2025) also found that CCN concentrations (accumulation mode particles) were associated with a decrease in echo top height, similar to the trends shown in Figure 5d. Other observational evidence of enervation is limited, but we do note that an enervation effect is consistent with some modeling studies. Fan et al. (2009) found a weakening in convective strength for greater concentrations of accumulation mode aerosols, particularly when vertical wind shear and environmental relative humidity are high (w>10m/s, RH from 500-900mb >60%). In the study, evaporative cooling and sublimation rates were enhanced under greater aerosol loading, which outweighed the boost to the storm's buoyancy from increased condensational heating. The increase in evaporation was proposed to be the result of either greater ventilation of cloud droplets, as discussed in (Khain, 2009), or higher entrainment rates.

Other aerosol invigoration studies have previously drawn a connection between stronger updrafts speeds and higher Aitken mode concentrations (van den Heever et al., 2006), accumulation mode concentrations (Blossey et al., 2018), or both (Tao et al., 2007; Wang, 2005) – the opposite of what we show in Figure 5d. However, in their model intercomparison study, Marinescu et al. (2021) showed a median model response of invigoration only below 7 km and a neutral to weak enervation response above 7 km. Similarly, Igel and van den Heever (2021) concluded that the sign of an aerosol invigoration response, particularly for warm-based storms, is a complex function of height and relies on whether changes in supersaturation, condensate loading, or unloaded fraction of condensate dominate. While Fan et al. (2013) included nucleation mode sizes in their analysis, their study similarly saw stronger vertical velocities with additional aerosol between 2 and 7 km, and a decrease in updraft speed above 8 km. As can be seen in Figure 3p, the CTRRMM window's median starting point is around 5 km, while the median endpoint of the window (Figure 3q) is near 9 km, with nearly 60% of endpoints occurring at or above 8 km. The altitudes over which the rise rates are valid, therefore, coincide with the heights at which enervation, in previous studies, seems most likely to occur. Thus, the trends displayed in Figure 5 are not necessarily inconsistent with previous studies which support aerosol invigoration.

To assess the relevance of a change in kinetic energy on a change in updraft speed, we note that $\frac{dKE}{dw} = w$, or $\Delta w \approx \frac{\Delta KE}{w}$. We expect this to be an upper limit on Δw since parcel theory typically overestimates updraft speed. Note also that the above equation states that the change in updraft speed depends not only on the change in kinetic energy but also on the strength of the storm. Table 1 reports the slope of the best fit lines seen in Figure 5 ($\Delta KE_{res}/\Delta N$) and the conversion of these slopes to estimated ranges of ΔCTRRMM/ΔN and ΔMAXW/ΔN. We use values of CTRRMM of 2 and 4 m/s based on Figure 3r as representative high and low values. Finally, to obtain ΔMAXW/ΔN, we use the relationship between CTRRMM and MAXW reported in Figure 2a. We stress that these are very rough estimates of the potential invigoration and enervation and intentionally only report estimates with one significant digit. Table 1 shows that the invigoration associated with the nanoscale particles is essentially negligible. Enervation is also small; the change in updraft speed likely does not exceed a few meters per second even for an increase of 1000 cm^{-3} of accumulation mode particles. Invigoration associated with the nucleation mode is the largest signal but still modest. We note that this slope is highly sensitive to the few highest nucleation mode concentration values in Figure 5b.

Table 1. Slope of the best fit lines, shown in Figure 5, for each aerosol mode. The corresponding change in updraft speed per 100 cm^{-3} additional aerosol particles is shown in the second column, for *w* of 2 and 4.5 m/s.

Aerosol Mode	$\Delta KE_{res}/\Delta N$ ($m^2 s^{-2}$ $(100\ cm^{-3})^{-1}$)	ΔCTRRMM/ΔN ($m\ s^{-1}$ $(100\ cm^{-3})^{-1}$)	ΔMAXW/ΔN ($m\ s^{-1}$ $(100\ cm^{-3})^{-1}$)
Nanoscale	0.033	~ 0.008 – 0.02	~ 0.04 – 0.08
Nucleation	0.25	~ 0.06 – 0.1	~ 0.3 – 0.6
Accumulation	-0.090	~ -0.02 – -0.05	~ -0.1 – -0.2

3.3 Environmental Conditions that Increase Statistical Significance

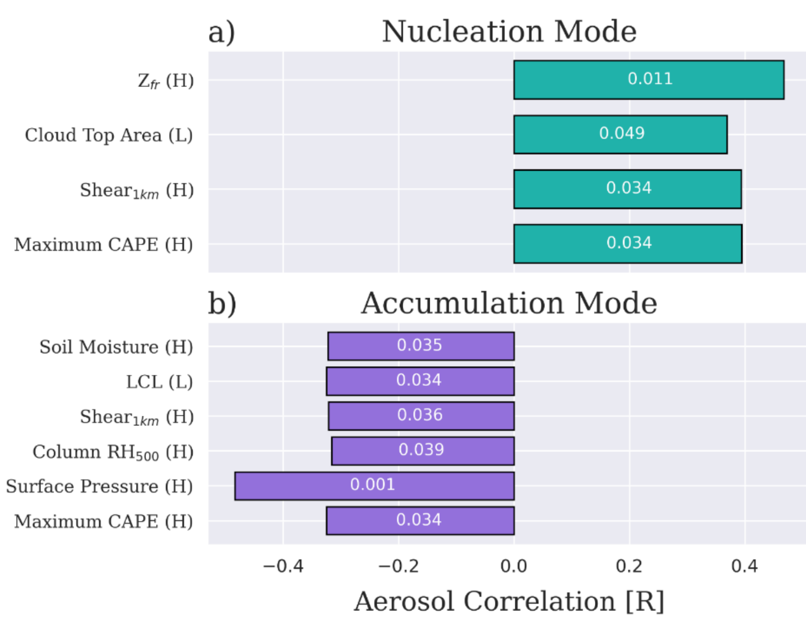

Figure 6. Bar graph of high (H) / low (L) subsets that show a significant association between ΔKE_{res} and number concentration at the 95% confidence level for nucleation mode particles (a)

and accumulation mode particles (b). The p-value for each correlation is displayed on the corresponding bar.

Although we do see a consistency between our results and previous works, none of the correlations in Figure 5b-d achieves statistical significance. Therefore, the ΔKE_{res} residuals are further subset by high and low values (top/bottom 50%) of the environmental predictors to understand the conditions under which an aerosol-updraft relationship becomes statistically relevant. Figure 6 shows the aerosol correlations with ΔKE_{res} for statistically significant subsets, using nucleation mode particles (top) and accumulation mode particles (bottom).

The ultrafine particle hypothesis of Fan et al. (2018) hinges on the ability to produce high supersaturation in the liquid-supporting regions of the storm to sustain secondary activation of nucleation mode particles. Fan et al. (2018) propose that the high supersaturation develops as a result of early warm-rain production (and thus requiring relatively low accumulation mode concentrations), but we note that Phillips (2022) shows that supersaturation can increase with height for strong updrafts in deep convection even before rain onset. As such, we might expect a stronger invigoration signal for storms with an extensive warm-phase region (to delay freezing) and environments that support strong updrafts. According to Figure 6a, high CAPE and high 0-1km shear environments provide a more significant association between convective intensity and nucleation mode particles. High values of both environmental properties favor stronger updrafts with the potential for higher supersaturation. (It should also be noted that there is a high overlap between the maximum CAPE and 0-1km shear subsets.) Figure 6a also shows a stronger association between convective intensity and nucleation mode particles for higher freezing heights, which we would expect to correlate with greater warm phase regions. (We similarly see an enhancement in the correlation with warmer cloud base temperatures, but the p-value of this correlation (0.052) is just over the statistical significance threshold.) All three strengthened associations then appear to be consistent with the Fan et al. (2018) hypothesis.

Figure 6a also suggests that storms with smaller cloud tops can see a boost in cloud top rise rates for greater concentrations of fine mode particles. This result is hard to interpret, as smaller cloud top areas are likely associated with narrower updrafts which are prone to dilution from the surrounding air (Morrison, 2017), reducing storm supersaturation. As such, we would not expect this subset to show a stronger relationship between nucleation mode concentrations and ΔKE_{res}. On the other hand, smaller cloud tops may also be associated with storms that loft less liquid water to the storm top where it is frozen to contribute to the anvil (Fan et al. 2013). If small anvils are associated with efficient precipitation processes, and since efficient precipitation production is required to obtain the high supersaturations required for secondary activation, then perhaps this result also supports the Fan et al. (2018) hypothesis. Ultimately, it is unclear whether or not the increased correlation in Figure 6a for smaller cloud top areas supports the hypothesis. Nevertheless, based on the analysis as a whole, we cannot conclude that the Fan et al. (2018) mechanism is insignificant.

Turning now to the conditions under which we could see enervation in the rise of the cloud top, Fan et al. (2009) suggest that entrainment can reduce convective intensity in polluted storms due to the narrowing of the cloud droplet spectra to smaller sizes, causing the smaller droplets to evaporate more readily in the drier, entrained air. Similarly, Peters et al. (2023) found that, due to its higher entrainment rate, a polluted parcel can see greater condensate and water vapor loss than that of its cleaner counterpart. The moisture loss due to increased dilution minimized the additional amount of latent heat that could be released during freezing in the polluted parcel and reduced the condensation/deposition rates. Hence, the polluted parcel's buoyancy is weakened, as the gain in temperature due to enhanced latent heat release is typically just enough to balance the drag on the buoyancy due to condensate loading (Grabowski and Morrison, 2020; Igel and van den Heever, 2021; Rosenfeld et al., 2008). Thus, we would expect to see a stronger enervation signal in environments which promote entrainment.

According to Figure 6b, storms with stronger low-level vertical wind shear and higher CAPE (again, these are highly correlated in our dataset) are more likely to see a decline in the rise of the cloud top with higher amounts of accumulation mode aerosols. Stronger vertical wind shear typically promotes greater lateral mixing across cloud boundaries due to enhanced turbulence generation (Stull, 1988), but a role of vertical wind shear in generating dynamic entrainment to ventilate the updraft has also been noted (Dahl, 2017; LeBel and Markowski, 2023). Polluted storms developing in environments with higher mid-level relative humidity may also slow, as seen in Figure 6b which could possibly be due to links between humidity and entrainment rates. A positive correlation between humidity and entrainment rate has been reported in recent studies (Bera and Prabha, 2019; Lu et al., 2018; Stirling and Stratton, 2012; Xu et al., 2021). Bera and Prabha (2019) showed that drier environments can increase the moisture flux between the boundary layer and the cloud layer, leading to stronger sub-cloud and cloud core updrafts that entrain less. Entrainment may also increase with relative humidity simply because only marginally diluted updrafts can survive in lower humidity environments (Lu et al., 2018; Stirling and Stratton, 2012). The increased likelihood of enervation in high column humidity and high low-level shear environments is also consistent with Fan et al. (2009), who explicitly tested the dependence of the invigoration/enervation strength on these two environmental properties.

Storms with lower cloud bases are also associated with a stronger enervation signal with increasing accumulation mode particle concentrations. Lower cloud bases may promote greater entrainment of the cloud core, as lower LCLs can result in narrower updraft widths (Mulholland et al., 2021). Storms with lower cloud bases may also experience more entrainment simply because their depth creates a greater extent over which entrainment can act. While entrainment-driven convective weakening appears plausible, the ECAPE parameter noticeably does not appear in Figure 6b. This may indicate that either the ECAPE quantity is not realistically capturing the entrainment rate of the storms or that entrainment is not the mechanism behind the enervation response. Without direct information on the entrainment rate or evaporation rates of the tracked storms, it is difficult to determine the mechanism responsible for the decreased ascent of the cloud tops. Nonetheless, the above subsets do appear to support the conclusions of both Fan et al. (2009) and Peters et al. (2023).

Finally, storms with higher surface pressures and higher soil moisture content may also increase the probability that storms are enervated by heightened accumulation mode concentrations. Higher surface pressures see the strongest and most significant association with CTRRMM in all of Figure 6, and it is the only subset that retains significance in Figure 6b if the ΔKE_{res} outlier is removed. However, the influence of higher surface pressures on the entrainment rates (or any other relevant process rates) of the storms is not immediately obvious. Similarly, while soil moisture has previously been recognized to be important to the strength of convective systems (Barton et al., 2025; Van Weverberg et al., 2010), its impact on the microphysical structure of clouds is not yet fully understood (Koukoula et al., 2019) and is particularly sensitive to its model representation (Massoud et al., 2025). Soil moisture is correlated with lower LCLs (perhaps by increasing latent heat fluxes), which is consistent with lower LCLs favoring more storm weakening. However, other links to storm strength are possible and its appearance in Figure 6 could also be spurious. Therefore, the results as they relate to both soil moisture and surface pressure in this work are difficult to interpret, and we leave it up to future study.

We emphasize that the above analysis does not demonstrate conclusive evidence of aerosol invigoration or enervation. We have by no means built a perfect, predictive model for CTRR, and our study certainly has limitations. For instance, we do not include the effects of cross-term interactions in the model. While we find no relationship between ΔKE_{res} and the predictors, interaction effects may still exist in ΔKE_{res}. Similarly, we could not account for all influences on CTRR, meaning that unattributed, environmental variables that correlate with the aerosol concentrations could result in an erroneous attribution of ΔKE_{res} to aerosol impacts. The focus on isolated, developing storms additionally limits our focus to the beginning stages of storm development, meaning invigoration that occurs later in the storm lifecycle is not addressed by our study. Furthermore, while we believe that most of the tracked storms form via free convection and within a well-mixed boundary layer (and that surface aerosol concentrations should therefore be indicative of the aerosol loading), we cannot rule out that heterogeneities in the vertical aerosol profile may exist and could alter our results. Therefore, the surface aerosol measurements at SGP may not always be representative of the aerosol conditions in the tracked storms. Finally, it is important to keep in mind that, with the above analysis, a large number of statistical tests are performed. As such, it is highly probable that one or more of our tests results in a spurious statistically significant signal. Because of these shortcomings, we urge caution in interpreting our results as definitive evidence of aerosol-induced invigoration or enervation. The correlations presented in this section only suggest, but do not definitively show, specific conditions under which aerosol invigoration may be feasibly detected observationally.

4 Conclusions

The goal of this study was to perform a robust, observational assessment of aerosol-induced invigoration on deep convective updraft speeds in the midlatitudes. We show a statistically significant, positive trend with ΔKE_{res} and increasing nanoscale particle concentrations at the 95% confidence level. When binned according to aerosol activation mode, our results suggest a dependence of the sign of the invigoration response on aerosol diameter. Multiple environmental subsets establish links to prior invigoration studies, including possible signatures of a secondary activation mechanism (Fan et al., 2018) and a weakening of convective strength with higher wind shear and greater mid-level relative humidities (Fan et al., 2009). Ultimately, our study does not definitively conclude whether aerosol-induced invigoration or enervation is present within the tracked storms. Instead, we show that both an invigoration and an enervation response is possible, that these results are largely qualitatively consistent with previous literature, and that the magnitude of the signals is likely modest at best. Our study suggests that invigoration is more likely under high CAPE conditions in storms with high freezing levels and high concentrations of the smallest activatable aerosol particles. It also suggests that enervation is more likely to occur in highly entraining environments associated with high concentrations of accumulation mode particles. In other words, the invigoration and enervation processes are not mutually exclusive. Future efforts in the field should, therefore, reject the framework of invigoration *or* enervation and instead focus on understanding the specific conditions under which each response may occur.

Appendix A: Environmental Variables

Table A1 lists the environmental variables used in the analysis, along with a description and any relevant statistics on its calculation. Table A2 lists the final predictor variables for each regression model, categorized by dependent variable and isolation criterion.

Table A1. Table with all relevant environmental variables in the first column, their descriptions in the second column, and specific details of their calculation, if applicable, in the third column.

Predictor Variable	Description	Calculation
AREA	Areal extent of the tracked storm	Tracked property
CAPE	Convective Available Potential Energy	Indexed at the location of the storm
MUCAPE	Most Unstable Convective Available Potential Energy	Domain averaged
ECAPE_FRAC	Fractional Entrained Convective Available Potential Energy	Calculated from (Peters et al., 2023), indexed at the location of the storm
ECAPE_RATE	Entrained Convective Available Potential Energy Rate	Calculated from (Peters, 2023), indexed at the location of the storm
MAXCAPE	Maximum Convective Available Potential Energy	Domain averaged
MEANCAPE	Mean Convective Available Potential Energy	Domain averaged
SHEAR1	One Kilometer Shear (0-1km)	Indexed at the location of the storm

SHEAR3	Three Kilometer Shear (0-3km)	Indexed at the location of the storm
SHEAR6	Six Kilometer Shear (0-6km)	Indexed at the location of the storm
RH_COLINT (600, 500, 400)	Column Integrated Relative Humidity	Indexed at the location of the storm, integrated from 700mb (600mb, 500mb, 400mb) to the top of the atmosphere
RH_DOINT (600, 500, 400)	Domain Integrated Relative Humidity Profile	Integrated over the domain from 700mb (600mb, 500mb, 400mb) to the top of the atmosphere
RH_DOAVG	Mean Relative Humidity	Domain averaged, from 700mb to the top of the atmosphere
RHSURF	Surface Relative Humidity	Domain averaged
PSURF	Surface Pressure	Domain averaged
TSURF	Surface Temperature	Domain averaged
LCL	Lifted Condensation Level	As in (Petty, 2008), eq. 7.30
EL	Equilibrium Level	Domain averaged
CIN	Convective Inhibition	Domain averaged
LI	Lifted Index	Domain averaged
SMOIST	Soil Moisture Availability	Domain averaged
FRZH	Height of the 0°C isotherm	Indexed at the location of the storm

Table A2. Table with final predictor variables for each regression model, grouped by dependent variable (rows) and isolation criterion (columns).

Regression Models	0.25°	0.30°	0.40°	0.50°
CTRRMM	MUCAPE, ECAPE_RATE, SHEAR6, RH_COLINT600, RH_COLINT500, RH_DOINT600, RH_DOAVG, PSURF, LCL, LI, FRZH	AREA, ECAPE_RATE, MAXCAPE, MEANCAPE, SHEAR3, SHEAR6, RH_COLINT500, RH_DOINT500, TSURF, EL, LI, FRZH	ECAPE_RATE, MAXCAPE, SHEAR3, RH_COLINT500, RH_DOINT400, RHSURF, EL, FRZH	ECAPE_FRAC, ECAPE_RATE, MAXCAPE, SHEAR3, RH_DOINT500, EL, CIN, FRZH
CTRRMAX	ECAPE_FRAC, ECAPE_RATE, MAXCAPE, MEANCAPE, RH_COLINT700, RH_COLINT600, RH_DOINT600, RH_DOINT500, RH_DOINT400, RH_DOAVG, LI	AREA, MUCAPE, ECAPE_FRAC, ECAPE_RATE, MAXCAPE, MEANCAPE, SHEAR6, RH_COLINT500, TSURF, LI	AREA, MUCAPE, ECAPE_FRAC, ECAPE_RATE, MEANCAPE, SHEAR3, RH_COLINT500, RHSURF, PSURF, EL, LI, SMOIST	ECAPE_FRAC, MEANCAPE, SHEAR3, RH_COLINT700, RH_COLINT500, RH_COLINT400, RH_DOINT700, EL

Appendix B: Regression Analysis

The following figures evaluate the statistical robustness of the 0.50° CTRRMM multiple regression model. Figure B1 compares $\Delta\mathbf{KE}_{\mathbf{res}}$ to the predicted cloud top rise rates of the model and indicates that the residuals are homoscedastic. Figure B2 also shows that the majority of the predictor variables are not correlated with the aerosol variables, except for two instances with nanoscale particle concentrations that will not weaken potential aerosol signals, as both relationships are positively correlated.

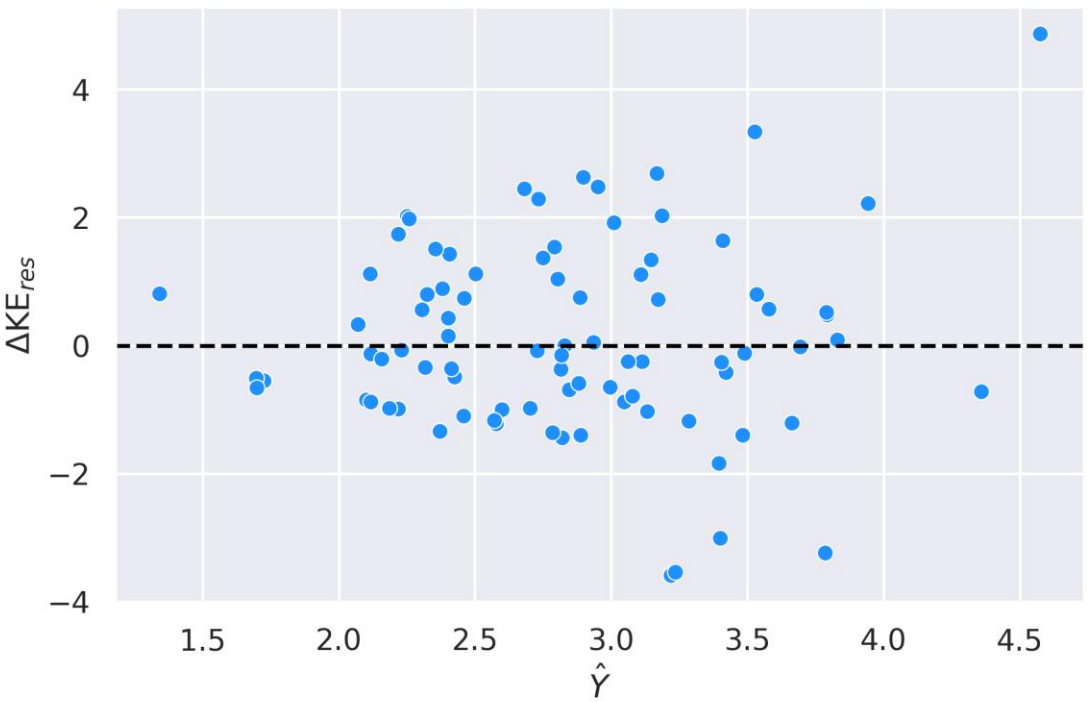

Figure B1. Residual plot of $\Delta\mathbf{KE_{res}}$ versus the predicted cloud top rise rates for the 0.50° CTRRMM regression model, with no systematic patterns in the residuals.

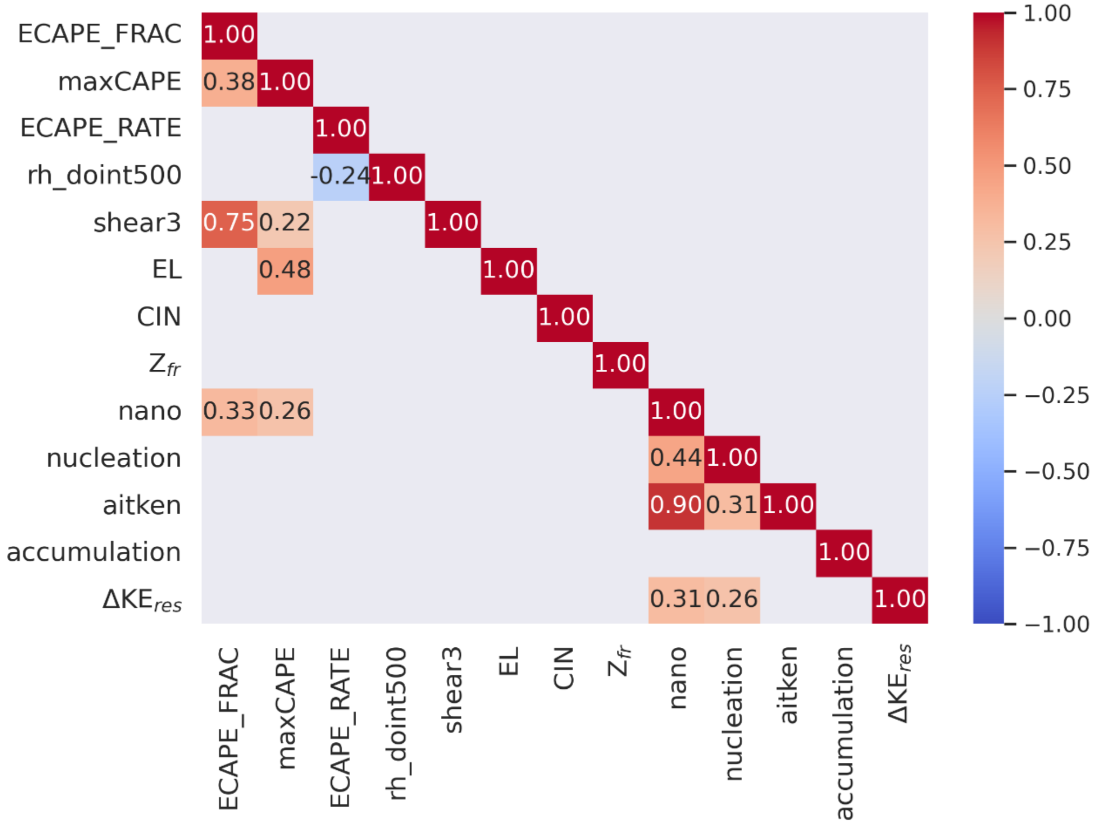

Figure B2. Correlation matrix between predictors, aerosol number concentrations, and $\mathbf{\Delta KE_{res}}$ for the 0.50° CTRRMM model.

Acknowledgments

This project was funded by the Department of Energy Atmospheric Science Research program under award DE-SC0022149. Support for HEP was also provided by the Atmospheric Science Graduate Group of University of California, Davis.

The authors would like to thank Corinna Hoose and Quentin Coopman for the generous use of their tracking algorithm. The authors also gratefully acknowledge the time and scientific contribution of the anonymous reviewers of the manuscript that led to the overall improvement of the quality and clarity of the paper.

A portion of this work used code generously provided by Brian Blaylock's Herbie and GOES-2-go python packages (https://doi.org/10.5281/zenodo.4567540).

Conflicts of Interest

The authors declare no conflicts of interest for this study.

Open Research

Data analysis scripts, including code to reproduce all figures, and processed data, including storm tracks, environmental data and aerosol data, are publicly available at: (Pimperl and Igel, 2026) 10.5281/zenodo.21229623.

References

Altaratz, O., Koren, I., Remer, L. A., and Hirsch, E.: Review: Cloud invigoration by aerosols—Coupling between microphysics and dynamics, Atmospheric Research, 140–141, 38–60, https://doi.org/10.1016/j.atmosres.2014.01.009, 2014.

Andreae, M. O., Rosenfeld, D., Artaxo, P., Costa, A. A., Frank, G. P., Longo, K. M., and Silva-Dias, M. A. F.: Smoking Rain Clouds over the Amazon, Science, 303, 1337–1342, https://doi.org/10.1126/science.1092779, 2004.

Anon: NOAA High-Resolution Rapid Refresh (HRRR) Model, n.d.

Baidu, M., Schwendike, J., Marsham, J. H., and Bain, C.: Effects of vertical wind shear on intensities of mesoscale convective systems over West and Central Africa, Atmospheric Science Letters, 23, e1094, https://doi.org/10.1002/asl.1094, 2022.

Barton, E. J., Klein, C., Taylor, C. M., Marsham, J., Parker, D. J., Maybee, B., Feng, Z., and Leung, L. R.: Soil moisture gradients strengthen mesoscale convective systems by increasing wind shear, Nat. Geosci., 18, 330–336, https://doi.org/10.1038/s41561-025-01666-8, 2025.

Bera, S. and Prabha, T. V.: Parameterization of Entrainment Rate and Mass Flux in Continental Cumulus Clouds: Inference From Large Eddy Simulation, JGR Atmospheres, 124, 13127–13139, https://doi.org/10.1029/2019JD031078, 2019.

Blaylock, B. K.: Herbie: Retrieve Numerical Weather Prediction Model Data, , https://doi.org/10.5281/ZENODO.4567540, 2026.

Blossey, P. N., Bretherton, C. S., Thornton, J. A., and Virts, K. S.: Locally Enhanced Aerosols Over a Shipping Lane Produce Convective Invigoration but Weak Overall Indirect Effects in Cloud-Resolving Simulations, Geophysical Research Letters, 45, 9305–9313, https://doi.org/10.1029/2018GL078682, 2018.

Coopman, Q., Riedi, J., Zeng, S., and Garrett, T. J.: Space-Based Analysis of the Cloud Thermodynamic Phase Transition for Varying Microphysical and Meteorological Regimes, Geophysical Research Letters, 47, e2020GL087122, https://doi.org/10.1029/2020GL087122, 2020.

Dahl, J. M. L.: Tilting of Horizontal Shear Vorticity and the Development of Updraft Rotation in Supercell Thunderstorms, Journal of the Atmospheric Sciences, 74, 2997–3020, https://doi.org/10.1175/JAS-D-17-0091.1, 2017.

Fan, J., Zhang, R., Li, G., and Tao, W.: Effects of aerosols and relative humidity on cumulus clouds, J. Geophys. Res., 112, 2006JD008136, https://doi.org/10.1029/2006JD008136, 2007.

Fan, J., Yuan, T., Comstock, J. M., Ghan, S., Khain, A., Leung, L. R., Li, Z., Martins, V. J., and Ovchinnikov, M.: Dominant role by vertical wind shear in regulating aerosol effects on deep convective clouds, J. Geophys. Res., 114, 2009JD012352, https://doi.org/10.1029/2009JD012352, 2009.

Fan, J., Leung, L. R., Rosenfeld, D., Chen, Q., Li, Z., Zhang, J., and Yan, H.: Microphysical effects determine macrophysical response for aerosol impacts on deep convective clouds, Proc. Natl. Acad. Sci. U.S.A., 110, https://doi.org/10.1073/pnas.1316830110, 2013.

Fan, J., Rosenfeld, D., Zhang, Y., Giangrande, S. E., Li, Z., Machado, L. A. T., Martin, S. T., Yang, Y., Wang, J., Artaxo, P., Barbosa, H. M. J., Braga, R. C., Comstock, J. M., Feng, Z., Gao, W., Gomes, H. B., Mei, F., Pöhlker, C., Pöhlker, M. L., Pöschl, U., and De Souza, R. A. F.: Substantial convection and precipitation enhancements by ultrafineaerosol particles, Science, 359, 411–418, https://doi.org/10.1126/science.aan8461, 2018.

Fan, J., Zhang, Y., Li, Z., Yan, H., Prabhakaran, T., Rosenfeld, D., and Khain, A.: Unveiling Aerosol Impacts on Deep Convective Clouds: Scientific Concept, Modeling, Observational Analysis, and Future Direction, JGR Atmospheres, 130, e2024JD041931, https://doi.org/10.1029/2024JD041931, 2025.

Grabowski, W. W.: Can the Impact of Aerosols on Deep Convection be Isolated from Meteorological Effects in Atmospheric Observations?, J. Atmos. Sci., 75, 3347–3363, https://doi.org/10.1175/JAS-D-18-0105.1, 2018.

Grabowski, W. W. and Morrison, H.: Untangling Microphysical Impacts on Deep Convection Applying a Novel Modeling Methodology. Part II: Double-Moment Microphysics, Journal of the Atmospheric Sciences, 73, 3749–3770, https://doi.org/10.1175/JAS-D-15-0367.1, 2016.

Grabowski, W. W. and Morrison, H.: Do Ultrafine Cloud Condensation Nuclei Invigorate Deep Convection?, Journal of the Atmospheric Sciences, 77, 2567–2583, https://doi.org/10.1175/JAS-D-20-0012.1, 2020.

Gustafson, W., Vogelmann, A., Cheng, X., Endo, S., Krishna, B., Li, Z., Toto, T., Xiao, H., and Johnson, K.: LASSO Data Bundles, https://doi.org/10.5439/1342961, 2017.

van den Heever, S. C., Carrió, G. G., Cotton, W. R., DeMott, P. J., and Prenni, A. J.: Impacts of Nucleating Aerosol on Florida Storms. Part I: Mesoscale Simulations, Journal of the Atmospheric Sciences, 63, 1752–1775, https://doi.org/10.1175/JAS3713.1, 2006.

Igel, A. L. and van den Heever, S. C.: Invigoration or Enervation of Convective Clouds by Aerosols?, Geophysical Research Letters, 48, e2021GL093804, https://doi.org/10.1029/2021GL093804, 2021.

Khain, A. P.: Notes on state-of-the-art investigations of aerosol effects on precipitation: a critical review, Environ. Res. Lett., 4, 015004, https://doi.org/10.1088/1748-9326/4/1/015004, 2009.

Koren, I., Altaratz, O., Remer, L. A., Feingold, G., Martins, J. V., and Heiblum, R. H.: Aerosol-induced intensification of rain from the tropics to the mid-latitudes, Nature Geosci, 5, 118–122, https://doi.org/10.1038/ngeo1364, 2012.

Koren, I., Dagan, G., and Altaratz, O.: From aerosol-limited to invigoration of warm convective clouds, Science, 344, 1143–1146, https://doi.org/10.1126/science.1252595, 2014.

Koukoula, M., Nikolopoulos, E. I., Kushta, J., Bartsotas, N. S., Kallos, G., and Anagnostou, E. N.: A Numerical Sensitivity Analysis of Soil Moisture Feedback on Convective Precipitation, Journal of Hydrometeorology, 20, 23–44, https://doi.org/10.1175/JHM-D-18-0134.1, 2019.

Kuang, C., Ermold, B., Singh, A., Salwen, C., and Hayes, C.: AOS: Scanning-Mobility Particle Sizer: nanoscale particles, https://doi.org/10.5439/1635016, 2021a.

Kuang, C., Singh, A., Howie, J., Salwen, C., and Hayes, C.: Scanning Mobility Particle Sizer, b1 level, https://doi.org/10.5439/1476898, 2021b.

LeBel, L. J. and Markowski, P. M.: An Analysis of the Impact of Vertical Wind Shear on Convection Initiation Using Large-Eddy Simulations: Importance of Wake Entrainment, Monthly Weather Review, 151, 1667–1688, https://doi.org/10.1175/MWR-D-22-0176.1, 2023.

Li, Z., Niu, F., Fan, J., Liu, Y., Rosenfeld, D., and Ding, Y.: Long-term impacts of aerosols on the vertical development of clouds and precipitation, Nature Geosci, 4, 888–894, https://doi.org/10.1038/ngeo1313, 2011.

Lin, J. C., Matsui, T., Pielke, R. A., and Kummerow, C.: Effects of biomass-burning-derived aerosols on precipitation and clouds in the Amazon Basin: a satellite-based empirical study, J. Geophys. Res., 111, 2005JD006884, https://doi.org/10.1029/2005JD006884, 2006.

Lu, C., Sun, C., Liu, Y., Zhang, G. J., Lin, Y., Gao, W., Niu, S., Yin, Y., Qiu, Y., and Jin, L.: Observational Relationship Between Entrainment Rate and Environmental Relative Humidity and Implications for Convection Parameterization, Geophysical Research Letters, 45, https://doi.org/10.1029/2018GL080264, 2018.

Marinescu, P. J., Van Den Heever, S. C., Heikenfeld, M., Barrett, A. I., Barthlott, C., Hoose, C., Fan, J., Fridlind, A. M., Matsui, T., Miltenberger, A. K., Stier, P., Vie, B., White, B. A., and Zhang, Y.: Impacts of Varying Concentrations of Cloud Condensation Nuclei on Deep Convective Cloud Updrafts—A Multimodel Assessment, Journal of the Atmospheric Sciences, 78, 1147–1172, https://doi.org/10.1175/JAS-D-20-0200.1, 2021.

Markowski, P. and Richardson, Y.: Mesoscale Meteorology in Midlatitudes, 1st ed., Wiley, https://doi.org/10.1002/9780470682104, 2010.

Massoud, E. C., Collier, N., Xu, M., Shi, M., and Hoffman, F. M.: Discrepancies in the Representation of Surface and Layered Soil Moisture in Earth System Models, https://doi.org/10.22541/essoar.174163272.24624137/v1, 10 March 2025.

Morrison, H.: An Analytic Description of the Structure and Evolution of Growing Deep Cumulus Updrafts, Journal of the Atmospheric Sciences, 74, 809–834, https://doi.org/10.1175/JAS-D-16-0234.1, 2017.

Mulholland, J. P., Peters, J. M., and Morrison, H.: How Does LCL Height Influence Deep Convective Updraft Width?, Geophysical Research Letters, 48, e2021GL093316, https://doi.org/10.1029/2021GL093316, 2021.

Öktem, R., Romps, D. M., and Varble, A. C.: No Warm-Phase Invigoration of Convection Detected during GoAmazon, Journal of the Atmospheric Sciences, 80, 2345–2364, https://doi.org/10.1175/JAS-D-22-0241.1, 2023.

Omar, A. H., Winker, D. M., Tackett, J. L., Giles, D. M., Kar, J., Liu, Z., Vaughan, M. A., Powell, K. A., and Trepte, C. R.: CALIOP and AERONET aerosol optical depth comparisons: One size fits none, JGR Atmospheres, 118, 4748–4766, https://doi.org/10.1002/jgrd.50330, 2013.

Peters, J.: ECAPE scripts, , 316374 Bytes, https://doi.org/10.6084/M9.FIGSHARE.21859818, 2023.

Peters, J. M., Lebo, Z. J., Chavas, D. R., and Su, C.: Entrainment Makes Pollution More Likely to Weaken Deep Convective Updrafts Than Invigorate Them, Geophysical Research Letters, 50, e2023GL103314, https://doi.org/10.1029/2023GL103314, 2023.

Petty, G. W.: A first course in atmospheric thermodynamics, Sundog Pub, Madison, Wis, 337 pp., 2008.

Phillips, V. T. J.: Theory of In-Cloud Activation of Aerosols and Microphysical Quasi-Equilibrium in a Deep Updraft, Journal of the Atmospheric Sciences, 79, 1865–1886, https://doi.org/10.1175/JAS-D-21-0176.1, 2022.

Pimperl, H. and Igel, A.: Aerosol, Storm, and Environmental Properties over the Southern Great Plains (2017-2024), https://doi.org/10.5281/ZENODO.21229623, 2026.

Romps, D. M., Latimer, K., Zhu, Q., Jurkat-Witschas, T., Mahnke, C., Prabhakaran, T., Weigel, R., and Wendisch, M.: Air Pollution Unable to Intensify Storms via Warm-Phase Invigoration, Geophysical Research Letters, 50, e2022GL100409, https://doi.org/10.1029/2022GL100409, 2023.

Rosenfeld, D., Lohmann, U., Raga, G. B., O’Dowd, C. D., Kulmala, M., Fuzzi, S., Reissell, A., and Andreae, M. O.: Flood or Drought: How Do Aerosols Affect Precipitation?, Science, 321, 1309–1313, https://doi.org/10.1126/science.1160606, 2008.

Schmit, T. J., Griffith, P., Gunshor, M. M., Daniels, J. M., Goodman, S. J., and Lebair, W. J.: A Closer Look at the ABI on the GOES-R Series, Bulletin of the American Meteorological Society, 98, 681–698, https://doi.org/10.1175/BAMS-D-15-00230.1, 2017.

Stirling, A. J. and Stratton, R. A.: Entrainment processes in the diurnal cycle of deep convection over land, Quart J Royal Meteoro Soc, 138, 1135–1149, https://doi.org/10.1002/qj.1868, 2012.

Storer, R. L., Van Den Heever, S. C., and L’Ecuyer, T. S.: Observations of aerosol-induced convective invigoration in the tropical east Atlantic, JGR Atmospheres, 119, 3963–3975, https://doi.org/10.1002/2013JD020272, 2014.

Stull, R. B. (Ed.): An Introduction to Boundary Layer Meteorology, Springer Netherlands, Dordrecht, https://doi.org/10.1007/978-94-009-3027-8, 1988.

Tao, W., Li, X., Khain, A., Matsui, T., Lang, S., and Simpson, J.: Role of atmospheric aerosol concentration on deep convective precipitation: Cloud-resolving model simulations, J. Geophys. Res., 112, 2007JD008728, https://doi.org/10.1029/2007JD008728, 2007.

Tao, W., Chen, J., Li, Z., Wang, C., and Zhang, C.: Impact of aerosols on convective clouds and precipitation, Reviews of Geophysics, 50, 2011RG000369, https://doi.org/10.1029/2011RG000369, 2012.

Van Weverberg, K., Van Lipzig, N. P. M., Delobbe, L., and Lauwaet, D.: Sensitivity of quantitative precipitation forecast to soil moisture initialization and microphysics parametrization, Q.J.R. Meteorol. Soc., 136, 978–996, https://doi.org/10.1002/qj.611, 2010.

Varble, A.: Erroneous Attribution of Deep Convective Invigoration to Aerosol Concentration, Journal of the Atmospheric Sciences, 75, 1351–1368, https://doi.org/10.1175/JAS-D-17-0217.1, 2018.

Varble, A. C., Igel, A. L., Morrison, H., Grabowski, W. W., and Lebo, Z. J.: Opinion: A critical evaluation of the evidence for aerosol invigoration of deep convection, Atmos. Chem. Phys., 23, 13791–13808, https://doi.org/10.5194/acp-23-13791-2023, 2023.

Veals, P. G., Varble, A. C., Russell, J. O. H., Hardin, J. C., and Zipser, E. J.: Indications of a Decrease in the Depth of Deep Convective Cores with Increasing Aerosol Concentration during the CACTI Campaign, Journal of the Atmospheric Sciences, 79, 705–722, https://doi.org/10.1175/JAS-D-21-0119.1, 2022.

Wang, C.: A modeling study of the response of tropical deep convection to the increase of cloud condensation nuclei concentration: 1. Dynamics and microphysics, J. Geophys. Res., 110, 2004JD005720, https://doi.org/10.1029/2004JD005720, 2005.

Wang, D., Kobrosly, R., Zhang, T., Subba, T., Van Den Heever, S., Gupta, S., and Jensen, M.: Aerosol impacts on isolated deep convection: findings from TRACER, Atmos. Chem. Phys., 25, 9295–9314, https://doi.org/10.5194/acp-25-9295-2025, 2025.

Xu, X., Sun, C., Lu, C., Liu, Y., Zhang, G. J., and Chen, Q.: Factors Affecting Entrainment Rate in Deep Convective Clouds and Parameterizations, JGR Atmospheres, 126, e2021JD034881, https://doi.org/10.1029/2021JD034881, 2021.